



Enzyme-catalyzed and binding reaction kinetics determined by titration calorimetry[☆]



Lee D. Hansen^{a,*}, Mark K. Transtrum^b, Colette Quinn^c, Neil Demarse^d

^a Department of Chemistry and Biochemistry, Brigham Young University, Provo, UT 84602, USA

^b Department of Physics & Astronomy, Brigham Young University, Provo, UT 84602, USA

^c TA Instruments, 890 W 410 N St., Lindon, UT 84042, USA

^d TA Instruments, 159 Lukens Drive, New Castle, DE 19720, USA

ARTICLE INFO

Article history:

Received 2 July 2015

Received in revised form 2 December 2015

Accepted 19 December 2015

Available online 22 December 2015

Keywords:

Calorimetry

ITC

Enzyme

Ligand binding

ABSTRACT

Background: Isothermal calorimetry allows monitoring of reaction rates via direct measurement of the rate of heat produced by the reaction. Calorimetry is one of very few techniques that can be used to measure rates without taking a derivative of the primary data. Because heat is a universal indicator of chemical reactions, calorimetry can be used to measure kinetics in opaque solutions, suspensions, and multiple phase systems and does not require chemical labeling. The only significant limitation of calorimetry for kinetic measurements is that the time constant of the reaction must be greater than the time constant of the calorimeter which can range from a few seconds to a few minutes. Calorimetry has the unique ability to provide both kinetic and thermodynamic data. **Scope of review:** This article describes the calorimetric methodology for determining reaction kinetics and reviews examples from recent literature that demonstrate applications of titration calorimetry to determine kinetics of enzyme-catalyzed and ligand binding reactions.

Major conclusions: A complete model for the temperature dependence of enzyme activity is presented. A previous method commonly used for blank corrections in determinations of equilibrium constants and enthalpy changes for binding reactions is shown to be subject to significant systematic error.

General significance: Methods for determination of the kinetics of enzyme-catalyzed reactions and for simultaneous determination of thermodynamics and kinetics of ligand binding reactions are reviewed. This article is part of a Special Issue entitled Microcalorimetry in the BioSciences – Principles and Applications, edited by Fadi Bou-Abdallah.

© 2015 Elsevier B.V. All rights reserved.

1. Introduction

Enzyme mechanisms and functions are a central theme in biochemistry, and the ability to characterize enzymes is increasingly important in industries where they are relied upon. Characterizing enzyme function and identifying changes in enzyme activity are essential in understanding the actions of pharmaceuticals. Characterizing enzyme function is also critical in the quest for renewable energy (e.g. to convert biomass into liquid fuels), in food production and processing, and in a variety of other industrial processes. Compared with spectroscopic methods, calorimetric methods do not require a chromophore and can be used in opaque media. Use of calorimetry as a universal method to measure the rates of enzyme binding reactions and enzyme-catalyzed

processes as a function of conditions of pH, concentrations, temperature, etc., make it an extremely powerful method to understand the precise conditions for specific enzyme activity.

Kinetic parameters obtained by ITC are used to address enzyme activities related to disease and general metabolism. Examples of enzyme activities investigated via ITC include *Trypanosoma cruzi* dihydroorotate dehydrogenase (Chagas disease) [1], *H. pylori* urease, HIV protease, heparinase I, acylase and subtilisin BPN', and hexokinase [2–4]. In their 1993 paper, Williams and Toone [4] make a legitimate point that crucial proteases and peptidases, responsible for regulating multiple metabolic functions, produce no native change detectable by traditional methods but can be addressed by ITC, and the function of amide hydrolysis is a viable target for a therapeutic attack.

Calorimetry has been used for rate measurements for more than 200 years. However, much of the information available on calorimetric methods for kinetics has not been applied to isothermal titration calorimetry (ITC). An isothermal titration calorimeter is but one particular type of calorimeter of several that can be used for kinetics. A literature review published in 2011 [5] found only 11 papers on kinetics in 2010 by use of the search terms “isothermal AND titration

[☆] This article is part of a Special Issue entitled Microcalorimetry in the BioSciences – Principles and Applications, edited by Fadi Bou-Abdallah.

* Corresponding author.

E-mail addresses: lee_hansen@byu.edu (L.D. Hansen), mktranstrum@byu.edu (M.K. Transtrum), cquinn@TAInstruments.com (C. Quinn), ndemarse@TAInstruments.com (N. Demarse).

AND calorimetry,” “ITC,” or isothermal titration calorimetry”; however, using the more general search terms “calorimet* and kinetic* and enzyme*” in Web of Science found 40 papers on enzyme kinetics published in 2010 and 630 published through 2014. The earliest was published in 1979. Researchers need to be aware of this when doing literature searches. Information gained from earlier calorimetric measurements of kinetics can be used to properly account for effects of calorimeter time constant and optimization for kinetic measurements. However, no suitable standard or agreed-on test reaction suitable for the kinetic methods reviewed here has been reported. Accuracy of results therefore depends on accurate calibration of calorimeters [6] and exact analysis of data.

2. Data produced by ITC

Kinetic data obtained by isothermal calorimetry are in the form of the rate of heat production, (dQ/dt) versus time, which is described by an equation of the form $dQ/dt = f(\text{time})$ and not by the more familiar $d(\text{product concentration})/dt = f(\text{reactant concentration})$. Also, since the response of heat conduction and power compensation calorimeters is relatively slow, the calorimetric equation must include the time constant, τ , except in the case of very slow reactions. In general, the time constant is included in the rate law describing the measured heat rate, $(dQ_{\text{measured}}/dt)$, as

$$(dQ_{\text{measured}}/dt)_t = \tau^{-1} \int_0^t e^{-(t-s)/\tau} (dQ_{\text{reaction}}/dt)_s ds. \quad (1)$$

In Eq. (1), the rate law for the heat rate from the chemical reaction is represented as $(dQ_{\text{reaction}}/dt)$. The measured heat rate is delayed due to the response time of the instrument (among other factors) and is calculated by integrating the heat generated at all previous times (denoted by the dummy variable s) with an exponential factor to account for the time delay. The time constant is included by means of the factor $\tau^{-1} \exp(t/\tau)$ where it is assumed that the calorimeter response is first order with respect to time, i.e., $\tau^{-1} \exp(-t/\tau)$ describes the instrument response [7]. This assumption is equivalent to the Tian equation, but note that here it is used as a fitting function, not as a correction done before data are fit to a chemical model. The Tian equation is

$$(dQ_{\text{reaction}}/dt) = (dQ_{\text{measured}}/dt)_t - \tau [d(dQ_{\text{measured}}/dt)_t/dt] \quad (2)$$

and Eq. (1) is the general solution to this function.

In Eq. (1), $(dQ_{\text{measured}}/dt)_t$ is the measured heat corrected for baseline such that $(dQ/dt)_0 = 0$. Note that τ must be included as a fitting parameter in data analysis since the value of τ changes with conditions; τ is not a constant for a given calorimeter [7,8]. Full description of kinetic data produced by ITC requires a two-part model, one part describing the characteristics of the calorimeter and another part describing the kinetics and thermodynamics of the chemical system. In this review, the kinetics of two types of reactions involving enzymes and other macromolecules are of interest; enzyme-catalyzed reactions and reactions in which a ligand molecule(s) is bound to the macromolecule with no further reaction.

In using calorimetry to make kinetic measurements, it must always be remembered that almost every process produces heat, and, if secondary chemistries are occurring along with the desired reaction, heat from these reactions will be detected in the total heat. Of these secondary chemistries, the biggest offenders are oxidation reactions from the presence of reducing agents such as dithiothreitol (DTT) in the reaction mixture.

3. Kinetics of enzyme-catalyzed reactions

The Michaelis–Menten/Briggs–Haldane (MM/BH) Eq. (2) describes most enzyme-catalyzed reaction kinetics.

$$dS/dt = -k_2[E_T][S]/(K_M + [S]) \quad (3)$$

In Eq. (3), $[S]$ is the free substrate concentration, $[E_T]$ is the total concentration of active enzyme, k_2 (or k_{cat}) is the rate constant, and K_M is the Michaelis–Menten, or mass action constant. The kinetics of an enzyme-catalyzed reaction can be obtained by two calorimetric procedures: single injection and multiple injection.

3.1. Multiple injection method

The multiple injection method is done by successive injections of substrate solution into an enzyme solution, see Fig. 1A and B. This method requires a priori knowledge of Δ_rH from a separate experiment and the time between injections must be $>6\tau$ to allow for calorimeter equilibration. Since a near steady state rate is achieved between injections, a time constant correction is unnecessary. The rate of substrate reaction, (dS/dt) , is obtained from Eq. (4), and the resulting rates can then be used to calculate $[S]_t$. K_M and k_2 can then be evaluated from one of the usual plots used for analysis of MM/BH kinetics, e.g. a plot of (dS/dt) versus S , see Fig. 1C.

$$(dS/dt)_t = (dQ_{\text{reaction}}/dt)_t / (-\Delta_rHV) = k_2[E_T][S]_t / (K_M + [S]_t) \quad (4)$$

In Eq. (4), $(dQ_{\text{reaction}}/dt)_t$ is the heat rate from the reaction of interest, Δ_rH is the enthalpy change for the reaction, V is the volume of the reaction vessel, and (dS/dt) is the rate of disappearance of the substrate. The sign convention used here is positive Q and negative Δ_rH for exothermic reactions. Likewise, the rate of production of product is

$$d(\text{product})/dt = (dQ_{\text{reaction}}/dt) / (-V\Delta_rH) \quad (5)$$

where (product) is the concentration of product.

In the multiple injection method, the rate and enthalpy are obtained in two separate experiments. For the determination of rate, $(dQ_{\text{reaction}}/dt)$, the substrate concentration in the injection syringe is typically 5–10 times greater than K_M . If K_M is unknown, a good starting point is high micromolar to low millimolar substrate. Steady state conditions are required after each injection and ideally $<5\%$ of the substrate is depleted between injections [2]. Experimentally, this requires working at a low enzyme concentration, delivering small injection volumes (2–5 μL), and using minimal time (2–4 minutes) between injections. If the substrate concentration is too high, $(dQ_{\text{reaction}}/dt)$ will not change between injections. If the substrate concentration is too low, $(dQ_{\text{reaction}}/dt)$ will not change after the first few injections. The enzyme in the cell is typically at picomolar to nanomolar concentration. If the enzyme concentration is too high, v_{max} will not be reached and $(dQ_{\text{reaction}}/dt)$ will change after every injection. v_{max} has been reached when additional aliquots of substrate do not yield an increase in $(dQ_{\text{reaction}}/dt)$. Under these conditions the concentration of substrate in the cell is greater than K_M . This condition occurs in the plateau region near the end of the plot in Fig. 1A. If a plateau is not reached, the substrate concentration needs to be increased. Note that rates are measured with respect to a baseline extrapolated from data collected before any injections occur. The rates are therefore subject to an unknown error from changes in the baseline from instrument drift or from changes in viscosity when substrate is injected or as the reaction progresses that cause a change in the stirring energy.

To determine Δ_rH , a second experiment with a low substrate concentration, $S \ll K_M$, is required, i.e. 100 times lower than used to determine the rate of enzyme activity. With an approximate 1000 times higher enzyme concentration, the substrate is quickly and completely

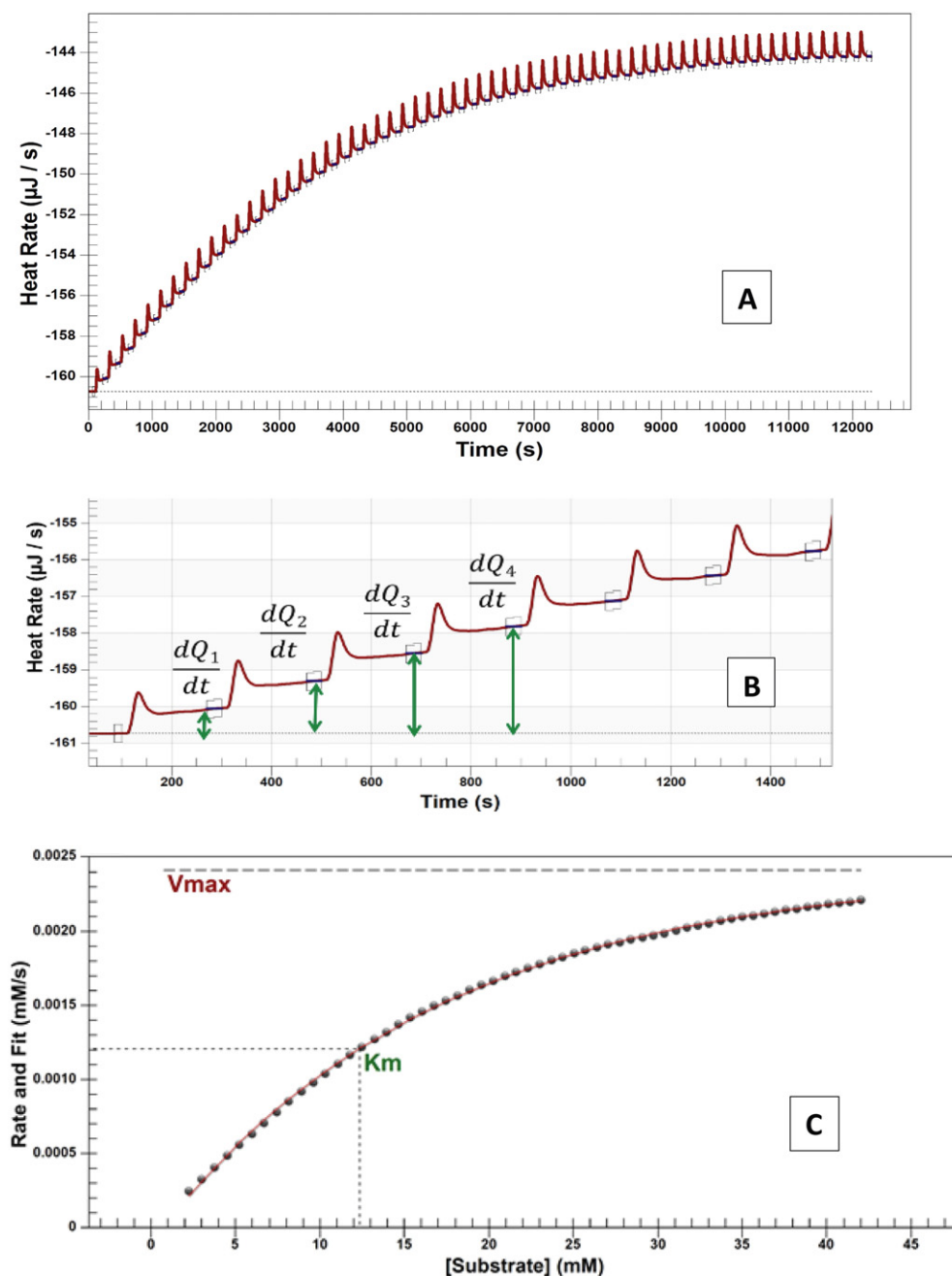


Fig. 1. A. Thermogram for substrate titrated into enzyme. 250 mM sucrose titrated into 5 nM invertase in 100 mM sodium acetate pH 5.65. Plotted as exotherm up. B. Magnified portion of A showing heat rate shift between injections. C. Michaelis–Menten plot of data from A.

converted into product. $\Delta_r H$ is calculated by dividing the integrated heat from the injection by the amount of substrate injected. At least three injections are recommended. The first injection is typically discarded because of diffusion during equilibration. A correction for heat of dilution of the titrant should be done if it is significant compared with the total heat for the injection.

To analyze data from the first experiment, plot $(dQ_{\text{reaction}}/dt)/(-V\Delta_r H)$ on the vertical axis and substrate concentration on the horizontal axis as in Fig. 1C. This plot is in the Michaelis–Menten form and can be analyzed by standard methods.

3.2. Single injection method

The single injection method usually requires less experimental time than the multiple injection method. In this method, values for τ , $\Delta_r H$,

k_2/K_M , and the baseline correction are obtained by fitting the data to the MM/BH model by one of the methods described below. Optimum conditions for data collection require that data are taken from both saturated, $[S] \gg K_M$, and unsaturated, $[S] \ll K_M$, conditions, Fig. 2. Furthermore, to separate reaction rates from the effects of calorimeter time constant on the data, the reactions must occur more slowly than the instrument response. Since the reaction must explore both the saturated and unsaturated regimes, the reaction is characterized by two effective reaction rates, $k_2[E_T]/K_M$ (unsaturated) and $k_2[E_T]/[S]$ (saturated). The calorimeter response rate ($1/\tau$) has to be faster than the slowest reaction rate, which occurs in the unsaturated regime, which in turn implies that $k_2[E_T]/K_M$ should be larger than $1/\tau$.

The fitting procedure can be validated by also determining $\Delta_r H$ from the total area under the curve and the amount of substrate in the reaction vessel. Typically, a moderate concentration of substrate (mM to

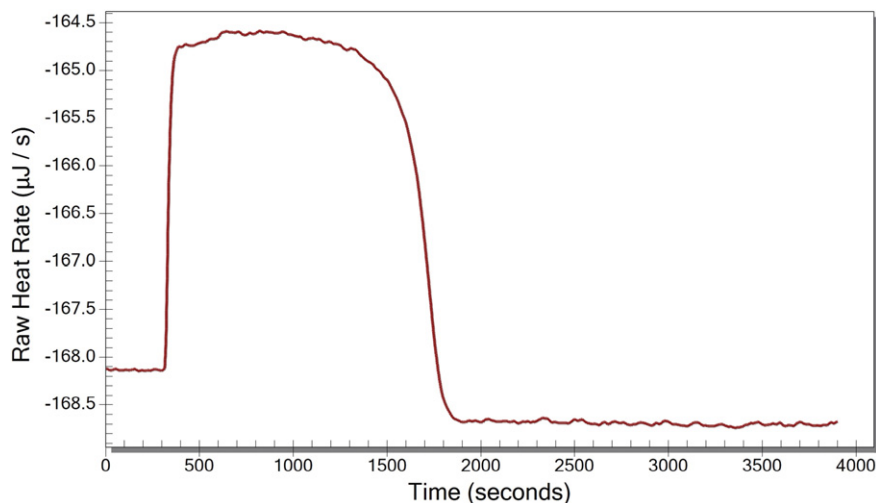


Fig. 2. Heat rate as a function of time for a single injection of 10 μL of 0.511 μM trypsin into 965 μL of 144 μM BAEE with both solutions in 200 mM Tris-HCl, pH 8.0, 50 mM CaCl₂, 0.2% PEG-2000. Plotted as exotherm up. The baseline shift is caused by a change in viscosity of the solution that decreases the heat rate from stirring.

μM) is in the reaction vessel and the concentration of enzyme in the syringe is μM to nM. The experiment can also be done with substrate in the syringe and enzyme in the reaction vessel. However, substrate solubility may require injection of a large volume with concomitant loss of a significant portion of the enzyme and a large heat of dilution. In either case, to avoid pre-reaction, a plug of buffer must be loaded into the end of the syringe needle, for example, 5 μL of enzyme with a 3 μL buffer plug necessitates an 8 μL injection.

A typical curve obtained by single injection of enzyme solution into substrate solution is shown in Fig. 2. If concentrations have been properly chosen, the early part of the curve of dQ_{measured}/dt versus time corresponds to enzyme saturated conditions (500–1300 s in Fig. 2) and less than saturating conditions occur during the decaying portion of the curve (1300–1900 s in Fig. 2). The baseline shift occurs on injection of the enzyme and is caused by a change in the heat rate from stirring. Note that the baseline should be interpolated between data collected before the injection and data collected after the reaction rate becomes negligible.

The instrument response time must be carefully considered in single injection experiments; the reaction completion time must be at least an order of magnitude greater than the instrument response time [8]. This can usually be achieved by increasing the substrate concentration. After correction for the heat of dilution of the titrant, the data are analyzed by fitting to the appropriate rate law for $(dQ_{\text{reaction}}/dt)$ in Eq. (1) to evaluate the time constant, parameters in the rate law, and the baseline heat rate. The initial data point where the analysis starts must be where $dQ_{\text{measured}}/dt = 0$. Assuming all substrate has been converted into product, the value of $\Delta_r H$ obtained from the curve fit can be verified by integrating the area under the entire curve and normalizing to the moles of substrate.

Analysis of single injection data requires converting the MM/BH equation into the calorimetric time function in Eq. (1), which is mathematically complex since there is no closed integral of the MM/BH equation. Two approaches to solve this problem have been used: a recursive calculation process [7] and integration of the MM/BH equation by means of the Lambert $W(x)$ or Omega function [9]. Integration with this function has not been used to analyze calorimetric data.

The recursive process (from [7] with minor changes) begins with the integrated rate law for the MM/BH equation

$$-K_M \ln[S] - [S] = k_2[E_T]t - K_M \ln[S]_0 - [S]_0, \quad (6)$$

where $[S]_0$ is the initial concentration of $[S]$. Although there is no explicit

expression for $S(t)$, S is uniquely defined for each t , so there is a unique inverse function

$$t(S) = -(1/k_2[E_T])[(S) - [S]_0 + K_M \ln([S]/[S]_0)], \quad (7)$$

which monotonically decreases from $[S]_0$ to 0. We exploit $t(S)$ to obtain $(dQ_{\text{reaction}}/dt)_t$ and $(dQ_{\text{measured}}/dt)_t$ for a sequence of times $t_0 < t_1 < \dots < t_N$ by the following algorithm:

1. Given values for $[E_T]$, k_2 , and K_M , discretize $[S]$ using a sequence of values $[S]_0 > [S]_1 > \dots > [S]_N = 0$ and compute $t(S)$ using Eq. (7).
2. Numerically invert $t(S)$ to obtain $[S](t)$, using an appropriate interpolation technique to obtain values of $[S](t)$ at each time $t_0 < t_1 < \dots < t_N$.
3. Use $[S](t)$ to obtain $(dQ_{\text{reaction}}/dt)_t$.

$$(dQ_{\text{reaction}}/dt)_t = -\Delta_r HV(dS/dt) = \Delta_r HVk_2[E_T][S]_t/(K_M + [S]_t), \quad (8)$$

where $(dQ_{\text{reaction}}/dt)_t$ is the heat rate from the reaction of interest, $\Delta_r H$ is the enthalpy change for the reaction, V is the volume of the reaction vessel, and (dS/dt) is the rate of disappearance of the substrate.

4. Use $(dQ_{\text{reaction}}/dt)_t$ from Eq. (8) in Eq. (1) to obtain $(dQ_{\text{measured}}/dt)_t$.
5. Choose better values of τ , k_2 , K_M , $\Delta_r H$ and, if necessary, the baseline heat rate and recycle the calculation until the best fit values of these parameters are reached.

4. Examples of studies of enzyme-catalyzed reaction kinetics

4.1. Enzyme-catalyzed reactions in single-phase systems

A paper by Aguirre et al. [10] provides an example of the extent of the results that can be obtained from analysis of kinetic data. This study obtained “Michaelis–Menten plots for the trypsin-catalyzed hydrolysis of several substrates at different temperatures (278–318K).” Data were collected with the single injection method at seven temperatures and under conditions where the reaction was sufficiently slow so that correction for instrument time constant was not required. Fig. 3 shows an example of the data from their study. Note that the data in Fig. 3 comply with the requirements for obtaining valid data by the single injection method, i.e. data from both the plateau and decaying regions of the curve are well-represented. For each substrate,

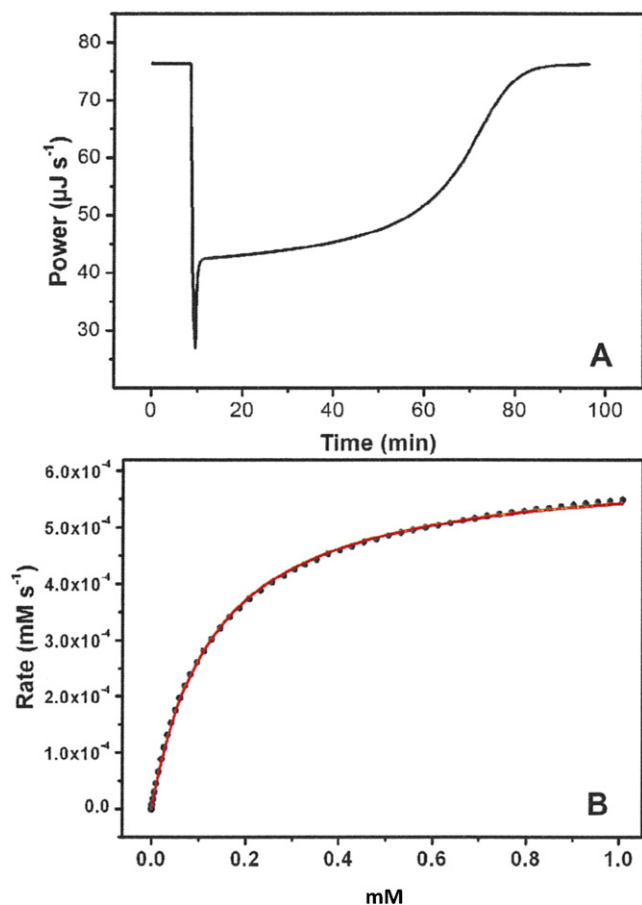


Fig. 3. Example of enzymatic activity of trypsin followed by ITC. (A) Raw data for thermal power change as a function of time. Plotted as exotherm down. (B) Reaction rates versus substrate concentration (mM) with the nonlinear least squares fit to the Michaelis–Menten equation to determine the steady-state kinetic parameters. Reproduced from reference [10] by permission.

a global fit of the data at all temperatures was done to obtain MM parameters and Arrhenius activation energies.

4.2. Kinetics of enzyme-catalyzed reactions in multi-phase systems

ITC is typically done by mixing enzyme and substrate solutions, but many systems of interest occur in suspensions, gels, and solids. A paper by Olsen et al. [11] describing enzymatic hydrolysis of lignocellulose (i.e., Avicel and pretreated corn stover) is an example of such a system. The high viscosity of the 29% solids in suspension precluded stirring and injection of titrant containing a cocktail of enzymes, so the “paste-like” mixture was prepared in the calorimeter vessel outside the calorimeter, inserted into a TAM III calorimeter, equilibrated for 30 minutes, and the heat rate followed for 18 hours. The experimental variable examined was the ratio of enzyme cocktail to substrate. The enzyme cocktail contained three enzyme activities, cellobiohydrolases (CBH) which attack the end of the polymer and create cellobiose, endoglycosidases (EG) which create ends by attacking the glucosidic bonds, and beta-glucosidases (BG) that convert cellobiose to glucose. Plots of heat rate versus time were fit with the sum of two exponentials in time, i.e. $dQ/dt = a \cdot \exp(-k_1 t) + b \cdot \exp(-k_2 t)$, and extent of reaction was determined from the total heat as a function of time as well as from chemical analyses for products of depolymerization of the cellulose.

Since a Michaelis–Menten rate law is not appropriate for such a system because the substrate is insoluble and heterogeneous, the data were analyzed in terms of the catalytic efficiency (i.e. rate/concentration of enzyme) and number of “attack points” on the substrate polymers.

Plots of conversion efficiency against time were used to gain insight into the action of the multi-enzyme system. The conversion efficiency was low at early stages of reaction because the ratio of enzyme to attack points was high. But as the endoglycosidases created more ends for the cellobiohydrolase to attack, conversion efficiency increased until it became limited by the enzyme concentration. The time required to reach a given conversion of substrate under identical substrate concentrations was either identical or increased in efficiency, which the authors concluded meant that the enzyme was not being inactivated over time as previously supposed. Since similar results were obtained with Avicel, pure cellulose, and corn stover, they also concluded that the enzymes were not inactivated by lignin.

Soil organic matter (SOM) mineralization to CO_2 is another multi-enzyme system of increasing interest because of the connection to climate change modeling. SOM originates from lignocellulose produced by plants and is solubilized by exoenzymes produced by soil microorganisms; a consortium of bacteria, archaea, and fungi. Rates of reaction are determined by the activity of the exoenzymes and the physical properties of the substrate carbon-containing materials. Measured heat rates include heat from metabolism as well as heat from hydrolysis of the polymeric substrates. Simultaneous measurements of CO_2 rates and metabolic heat rates provide values for the calorimetric ratio which provides information on the substrate being metabolized. Since the temperature dependence of the rates of these processes are of great interest, methods have been developed for automated calorimetric determination of the temperature dependence with a step-scan in a TAM III calorimeter [12].

Since metabolism is catalyzed by enzymes, the metabolic rate of organisms, tissues, and cells fits within the subject of this paper. Metabolic heat rates of organisms from large mammals to microorganisms have been measured by direct calorimetry [13]. Such measurements are of interest for a wide variety of reasons from feed conversion efficiency in farmed animals to responses of poikilotherms to climate change. Direct calorimetry has an important application in determination of the effects of temperature on metabolic rates and efficiencies [14]. Most of these studies obviously require use of calorimeters with reaction vessels that are accessible by more than a narrow tube as is the case in most ITCs. However, metabolic heat rates in microbial suspensions that do not settle can be obtained with a detection limit of ± 25 nW/mL in calorimeters with fixed cells by removing the stirrer [15]. Stirring is the major source of thermal noise in these calorimeters.

5. Temperature dependence of kinetics of enzyme-catalyzed reactions

Most reports on the temperature sensitivity of enzyme catalyzed reactions model the results by replacing k_2 in Eq. (3) with an Arrhenius function, i.e. $k_2 = A e^{-E_a/RT}$, where E_a is regarded simply as an empirical fitting parameter. However, a deeper understanding of the temperature dependence can be gained by realizing there are two sources of temperature dependence in enzyme-catalyzed reactions; the rate of diffusion of substrate into the active site of the enzyme, which is correctly described by an Arrhenius function, and the activity of the enzyme, which does not follow an Arrhenius temperature dependence. Enzyme activity increases exponentially at low temperature, but as temperature rises, a plot of activity versus temperature goes through an inflection point, reaches a maximum, and then declines at higher temperature, e.g. see [16,17]. Thus, activity measured only over the low temperature range can be fit with an Arrhenius function, but the curve of activity versus temperature diverges from the Arrhenius function as temperatures approach and exceed the temperature of maximum activity.

The Arrhenius function, Eq. (8), describes the change with temperature in the number of substrate molecules with sufficient translational and rotational energy, E_a , to bind to the enzyme.

$$dn/dt = A \cdot \exp(-E_a/RT) \quad (9)$$

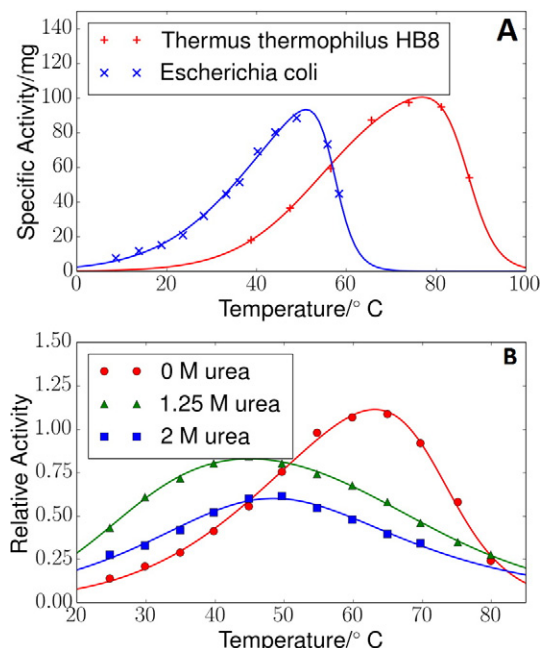


Fig. 4. Fits of enzyme activity versus temperature (solid lines) with Eq. (14). (A) shows “specific activity temperature profiles of *E. coli* (X) and *Th. thermophilus* (+) IPMDHs in 0.3 M and 1.0 M KCl, respectively, in 20 mM potassium phosphate buffer pH 7.6 containing 0.2 mM MnCl_2 .” DSC data show that the thermal signal from melting or unfolding of the *E. coli* enzyme begins at 64 °C and of the *Th. thermophilus* at 80 °C. [16] (B) shows “Normalized activity . . . of NADH oxidase . . . measured in 50 mM phosphate buffer, pH 7.2, in the absence of urea, 1.25 M urea, and 2.0 M urea.” Ellipticity at 220 nm shows that melting or unfolding of the enzyme begins at 76 °C in 0 M urea, at 78 °C in 2.6 M urea and at 81 °C in 1.3 M urea. [17]

A is a frequency factor related to the probability that a substrate molecule is correctly oriented to diffuse into the active site of the enzyme. R is the gas constant and T is the Kelvin temperature.

Because temperature plays an integral role in enzyme-substrate conjugation, enzyme activity can vary with temperature and have a greater temperature dependence than diffusion. Enzymes are typically inactive at low temperatures. As temperature increases, catalytic activity increases. But at higher temperatures, catalytic activity decreases with further increases in temperature. This temperature dependence can be described by the partition function for a three state equilibrium model of enzyme activity. Consider the following equilibria among three states of an enzyme,

$$E_L = E_A = E_H \quad (10)$$

E_L is the low-temperature, inactive state(s), E_A is the active state(s), and E_H is the high-temperature inactive state(s). Defining n_A as the number of enzyme molecules in the active state and N as the total number of

enzyme molecules, the fraction of molecules in the active state is n_A/N and $0 < n_A/N < 1$. Expressing this fraction in terms of the canonical partition function gives

$$n_A/N = \left(g_A e^{-\varepsilon_A/RT} \right) / \left(g_L e^{-\varepsilon_L/RT} + g_A e^{-\varepsilon_A/RT} + g_H e^{-\varepsilon_H/RT} \right), \quad (11)$$

where g is the degeneracy of each state, ε is the energy of each state, R is the gas constant, (i.e. Boltzmann's constant on a molar scale), and T is absolute temperature. Note that L, A, and H are indices in the exponents, not multipliers. Defining $g_L = 1$ and $\varepsilon_L = 0$, i.e. defining subscript L as the reference state, and dividing the numerator and denominator by $g_L e^{-\varepsilon_L/RT}$, then gives

$$n_A/N = \left(\Delta g_A e^{-\Delta\varepsilon_A/RT} \right) / \left(1 + \Delta g_A e^{-\Delta\varepsilon_A/RT} + \Delta g_H e^{-\Delta\varepsilon_H/RT} \right), \quad (12)$$

where g and ε are now relative to the low temperature state. (Eq. (12) has been commonly applied to describe the melting or unfolding of proteins in solution, e.g. [18], but is used here to describe the dependence of enzyme activity on temperature.)

Combining Eq. (12) with the Arrhenius function, Eq. (9), gives

$$dS/dt = \left(A \Delta g_A e^{-(E_a + \Delta\varepsilon_A)/RT} \right) / \left(1 + \Delta g_A e^{-\Delta\varepsilon_A/RT} + \Delta g_H e^{-\Delta\varepsilon_H/RT} \right) \quad (13)$$

Note that the numerator of Eq. (13) is equivalent to the Arrhenius function, but the meaning is different. The function in the denominator causes dS/dt to decrease at higher temperatures. Thus, as temperatures approach the temperature of maximum activity, the function in Eq. (13) behaves entirely different than the Arrhenius function. The two functions just happen to be similar at temperatures in the low end of the range of temperatures where the enzyme is partially active.

The data in Fig. 4 show that the function that describes enzyme activity as a function of temperature must begin near zero at a sufficiently low temperature, rise exponentially until it goes through an inflection point, increase up to a maximum, and then decrease to zero at higher temperature where the enzyme is completely inactive, but possibly not unfolded [16,17]. Fig. 4A and B show data from references [16] and [17] and lines fit to the data with Eq. (13). The parameters from the fits are given in Table 1. Data in these references [16] and [17] also show that the decline in enzyme activity at temperatures above the optimum is not caused by melting or unfolding of the tertiary structure of the enzyme. These findings indicate that enzymes have to have just the right amount of conformational freedom to be active, low temperatures restrict conformational freedom, and high temperatures lead to loosening of enzyme structure with consequent loss of activity.

Table 1

Parameters from fitting enzyme activity data in Fig. 4 to Eq. (13), $dS/dt = A \Delta g_A \exp(-(E_a + \Delta\varepsilon_A)/RT) / (1 + \Delta g_A e^{-\Delta\varepsilon_A/RT} + \Delta g_H e^{-\Delta\varepsilon_H/RT})$.

Enzyme	$\ln C^a$	E_a/eV	$\Delta\varepsilon_A/\text{eV}$	$\ln \Delta g_A$	$\Delta\varepsilon_H/\text{eV}$	$\ln \Delta g_H$
IPMDH from <i>E. coli</i>	36.4	3.1e-4	0.90	31.6	4.5	146.3
IPMDH from <i>Th. thermophilus</i>	30.7	5.7e-6	0.70	25.6	4.5	160.3
NADH oxidase from <i>Th. thermophilus</i> in 0 M urea	27.7	3.6e-6	0.76	27.1	2.9	99.6
NADH oxidase from <i>Th. thermophilus</i> in 1.25 M urea	40.3	3.2e-5	1.0	40.3	1.9	70.0
NADH oxidase from <i>Th. thermophilus</i> in 2.0 M urea ^a	18.6	1.7e-5	0.51	5.8	1.1	38.4

^a The model exhibits a correlation between the scaling factor A and the state degeneracies Δg_A and Δg_H . This correlation is problematic when the activation curve is relatively flat, as in the 2 M urea case. For these data, the best fit occurs for a very large value of A with relatively small values for the degeneracies. These extreme parameter values are a consequence of correlations among the fitted parameters and are likely not meaningful for interpretation of enzyme conformational states. We therefore report values for the combination $C = A \Delta g_A$.

6. Kinetics of binding reactions

The Ng Eq. (15)[19] includes all of the common rate laws used to describe binding reactions.

$$dx/dt = k(x)^m(1-x)^n \quad (15)$$

In Eq. (15), x is a concentration, molar amount, or fraction reacted; k is the rate constant; and m and n are mechanism-dependent parameters. Most of the common rate laws can be derived from the Ng equation by selecting integer values for m and n , and these rate laws are easily converted into a function of time, i.e. to yield an explicit function $x(t)$ [7]. In general, the incomplete beta function can be used to integrate the Ng equation [7] to provide an equation for the rate as a function of time. The single injection method has been widely used to determine kinetics of many different types of reactions and has been particularly effective in measuring rates of very slow reactions [20,21].

In 2007, Egawa et al. [22] proposed making use of the kinetic information contained in a series of incremental injections (i.e., an ITC titration) to determine the “association and dissociation rate constants of reversible bimolecular reactions.” Egawa et al. lists 5 steps in their data analysis (apparently done after correction of the measured curve for the calorimeter time constant with the integrated form of the Tian equation): 1) determine K_d and concentrations from the curve of the integrated data; 2) calculate a criterion parameter r' ; 3) based on r' , determine which of the peaks in the titration curve are described by a single-exponential fit; 4) determine the overall rate constant from the exponential decay curve; and 5) separate the overall rate constant into k_{for} and k_{rev} , respectively, from the slope and intercept of a plot of the overall rate constant versus the sum of the free concentrations of the two reactants. In 2012, Burnouf et al. [23] described a “new method for obtaining joint thermodynamic and kinetic data by isothermal titration calorimetry” and software (AFFINImeter) for data analysis by this method has recently become available [24]. The Burnouf et al. supplementary gives 5 steps in their data analysis: 1) adopt a kinetic model for the chemical reactions, 2) calculate an ideal ITC curve (we assume this means describing only the heat rate from the chemical reactions using K_d and $\Delta_r H$ determined from the curve of integrated data), 3) use the previously determined value of τ in the integrated Tian equation to correct for instrument response, 4) calculate a corrected curve, and 5) compare the corrected curve with the measured curve (which we assume includes minimization to find the best fit parameters). Burnouf et al. [23] also describes a global fit of titrations performed at different temperatures using the Arrhenius function to model two kinetic constants and an extended van't Hoff equation to model the temperature dependencies of K_d and $\Delta_r H$. The temperature-dependent data set is further interpreted with a two-step mechanism involving ligand binding followed by RNA folding.

Both Egawa et al. and Burnouf et al. proposed to determine the time constant of the calorimeter in a separate experiment by an impulse of heat from an electric heater or by an injection of methanol into water [22,23]. However, this procedure only gives the lower limit for τ [8] because τ depends on the composition (or thermal conductivity) and mixing time of the solution in the reaction vessel as well as the time constant in the control loop of power compensation instruments, or on the sensor time constant in heat conduction calorimeters. Since τ can vary from experiment to experiment and possibly from injection to injection, τ should be treated as a fitting parameter during the data analysis. To determine the significance of the error in results caused by errors in τ , we independently developed a model as described below and analyzed a set of data with our code. The data set was collected and analyzed by Lynn DeLeeuw and Jonathan B. Chaires at the University of Louisville using Origin and AFFINImeter software. The data set was initially provided to us with no indication of the identity of the reactants or the AFFINImeter report that are given in Supplements 1 and 2.

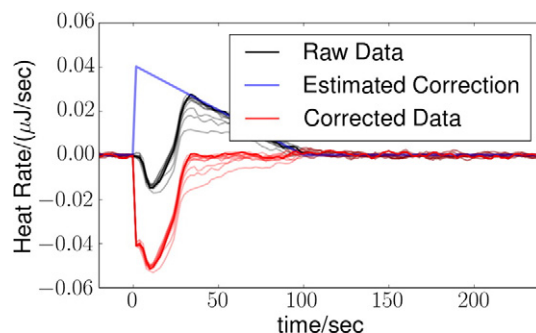


Fig. 5. Method of correction for the blank. Plotted as exotherm down. The blank correction, dQ_{cell}/dt , was determined as a linear backward extrapolation of the endotherm to the beginning of the injection. The last ten injections of the titration are plotted on a common horizontal axis.

The following Eqs. (16)–(20) provide a global model for analysis of this data set.



M is the macromolecule in the reaction vessel, and L is the ligand in the titrant.

Changes in the concentrations of M , L , and ML during and after each injection are described by three differential equations where $(dV_{\text{titrant}}/dt) > 0$ only when the buret is actually delivering titrant.

$$d[M]/dt = (-k_{\text{for}}[M][L] + k_{\text{rev}}[ML]) - ([M]/V_{\text{cell}})(dV_{\text{titrant}}/dt) \quad (17)$$

$$d[L]/dt = (-k_{\text{for}}[M][L] + k_{\text{rev}}[ML]) + ((C_{\text{titrant}} - [L])/V_{\text{cell}}) \times (dV_{\text{titrant}}/dt) \quad (18)$$

$$d[ML]/dt = (+k_{\text{for}}[M][L] - k_{\text{rev}}[ML]) - ([ML]/V_{\text{cell}})(dV_{\text{titrant}}/dt) \quad (19)$$

The concentration of titrant in the buret is denoted by C_{titrant} . Note that these last three equations include k_{for} , k_{rev} , and implicitly, $\Delta_r H$ and n as fitting parameters where n is the ratio of binding sites calculated from the data to the concentration of binding sites calculated from the solution composition. The calorimeter time constant, τ , is assumed to follow the function in Eq. (1) and τ can also be used as a fitting parameter. Two corrections must be made to the data, a baseline correction, $(dQ/dt)_{\text{baseline}}$, must be subtracted from the data, so that

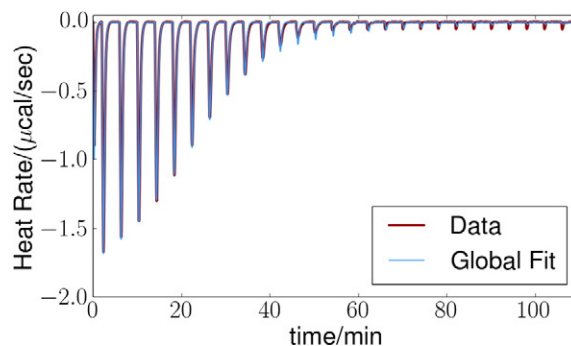


Fig. 6. Global fit of blank-corrected data with 6 parameters, k_{for} , k_{rev} , $\Delta_r H$, n , τ , and dQ_{baseline}/dt where dQ_{baseline}/dt is the baseline heat rate between injections. K_d is implicitly estimated as $k_{\text{rev}}/k_{\text{for}}$. Plotted as exotherm down. Input data were concentration of L in the buret (0.79 mM), initial concentration of M in the reaction vessel (0.05 mM sites), reaction vessel volume (1.4151 mL), and the buret delivery rate was 0.5 $\mu\text{L/s}$. The titration consisted of a first injection of 5 μL with subsequent injections of 10 μL at 240 second intervals. The $(dQ_{\text{measured}}/dt)_t$ data are given in Supplement 1.

Table 2
Comparison of results from different methods applied to a titration with 10 μL injections of 0.79 mM ligand into 1.415 mL of 0.05 mM DNA sites. Statistical uncertainties in the global fit are given as 95% confidence intervals.

Method	k_{for} , $\text{mM}^{-1} \text{s}^{-1}$	k_{rev} , s^{-1}	K_{d} , μM	$-\Delta_{\text{r}}H$, kJ mol^{-1}	n	dQ_{baseline}/dt , μW	Time constant, τ , seconds
Global fit ^a	3.09 ± 0.42	0.0079 ± 0.0014	2.56 ± 0.29	29.2 ± 0.8	0.851 ± 0.018	0.006 ± 0.010	12.5 ± 1.4
K_{d} and $\Delta_{\text{r}}H$ determined with NanoAnalyze ^b	–	–	2.50 ± 0.24	30.4 ± 0.5	0.847 ± 0.01	–	–
Global fit with $n = 0.847$	3.13	0.0081	2.59	29.3	–	0.006	12.6
AFFINmeter with $\tau = 13 \text{ s}^c$	3.55 ± 0.06	0.0073 ± 0.0001	2.05 ± 0.03	28.9 ± 0.1	0.874	–	–
Global fit with $n = 0.874$, $\tau = 13 \text{ s}$	3.19	0.0076	2.38	28.7	–	0.025	–
K_{d} and $\Delta_{\text{r}}H$ determined with Origin ^b	–	–	3.40 ± 0.25	34.8 ± 0.5	0.811 ± 0.009	–	–

^a Uncertainties are 95% confidence limit.

^b Uncertainties are 68% confidence limit.

^c The AFFINmeter report does not state the meaning of these uncertainties. These uncertainties do not account for correlations among kinetic parameters and τ , resulting in greatly underestimated uncertainties relative to the global fit in the first row.

$dQ_{\text{measured}}/dt = 0$ just before the next injection begins, and a blank correction for the heat of dilution of the titrant, Q_{dil} (or (dQ_{dil}/dt)), must be subtracted from each peak in the curve. The data analysis thus must arrive at values of $(dQ/dt)_{\text{baseline}}$, Q_{dil} , K_{d} , $\Delta_{\text{r}}H$, k_{for} , k_{rev} , τ , and n. To obtain K_{d} , we assume the dissociation constant, K_{d} , is related to the rate constants, k_{rev} and k_{for} , by

$$K_{\text{d}} = k_{\text{rev}}/k_{\text{for}} = [M][L]/[ML]. \quad (20)$$

Because the system is overdetermined, there are several options as to the sequence of steps used to analyze the data. We used the following sequence:

1. Correct for the heat of mixing of the titrant, Q_{dil} , by subtracting a constant, or a function, dQ_{dil}/dt , from each peak in the curve.
2. Correct for baseline by subtracting a constant $(dQ/dt)_{\text{baseline}}$, or a polynomial function of $(dQ/dt)_{\text{baseline}}$, from each data point.
3. Assume values for $\Delta_{\text{r}}H$, k_{for} , k_{rev} , τ , and n.
4. Compute $d[M]/dt$, $d[L]/dt$, and $d[ML]/dt$.
5. Compute $(dQ_{\text{reaction}}/dt)_t = \Delta_{\text{r}}H V_{\text{cell}}(k_{\text{for}}[ML] - k_{\text{rev}}[ML])$.
6. Compute $(dQ_{\text{measured}}/dt)_t$ from Eq. (1) and compare with the experimental curve of $(dQ_{\text{measured}}/dt)_t$ to select better values of the fitted parameters.

7. Cycle to step 2 until best fit values of $(dQ/dt)_{\text{baseline}}$, $\Delta_{\text{r}}H$, k_{for} , k_{rev} , τ , and n are obtained for all injections in the titration.
8. Compute $K_{\text{d}} = k_{\text{rev}}/k_{\text{for}}$.

In our application of this procedure, $(dQ/dt)_{\text{baseline}}$, $\Delta_{\text{r}}H$, k_{for} , k_{rev} , n, and τ were all used as fitting parameters. Input data were concentration of L in the buret, initial concentration of M in the reaction vessel, reaction vessel volume, buret delivery rate, injection volumes, time interval between injections, and $(dQ_{\text{measured}}/dt)_t$. Note that this procedure differs from the procedures used by Egawa et al. [22] and Burnouf et al. [23] in that our procedure does not make use of the integrated data to determine K_{d} and $\Delta_{\text{r}}H$, thus leaving this procedure as an independent means of verifying the results from the kinetic analysis. Our procedure also treats $(dQ/dt)_{\text{baseline}}$ and τ as fitting parameters instead of using an *a priori* evaluation of the values of these parameters.

The correction for Q_{dil} was first done by integrating the peaks of the last few data points and subtracting the average result from all the previous peaks. However, despite attempts to manually adjust the value of Q_{dil} , the curve calculated with the model always showed small exothermic peaks for each of the injections in the tail of the curve and poor fitting of the early peaks in the curve. These peaks are the result of two processes. Because the reaction is incomplete at the end point, some unreacted M remains, and a significant amount of the forward

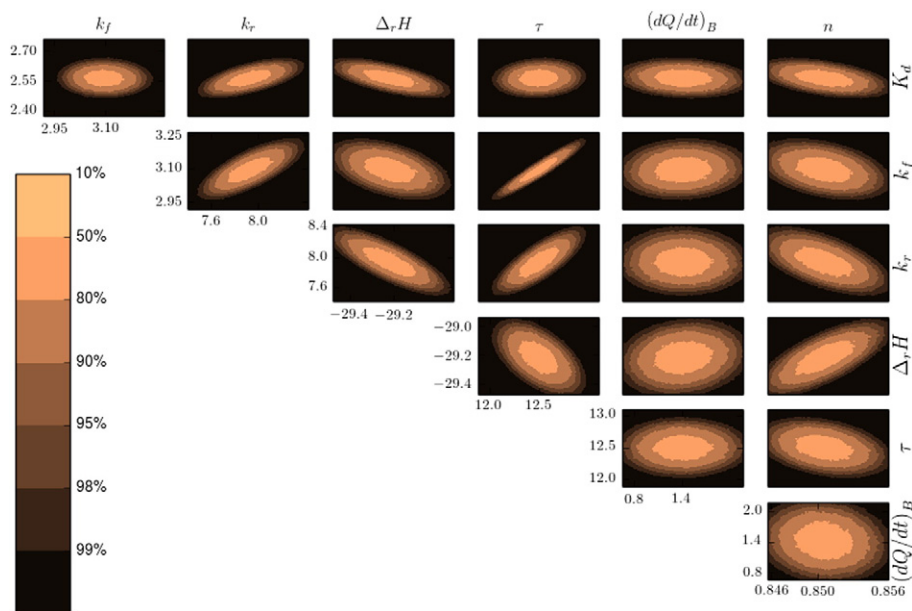


Fig. 7. Joint confidence regions showing the pairwise correlations among the fitting parameters. K_{d} is given in units of μM , k_{f} in mM s^{-1} , k_{r} in ms^{-1} , $\Delta_{\text{r}}H$ in kJ mol^{-1} , τ in seconds, n is dimensionless, and $(dQ/dt)_{\text{B}}$ (or dQ_{baseline}/dt) in nW. Confidence regions correspond to level sets of chi-squared cost. The percentage levels are $100(1-\alpha)\%$ confidence levels as generated from a standard F-test. The strongest correlations are among τ and the kinetic parameters k_{f} and k_{r} , indicating the importance of including τ as a fitting parameter. Another notable correlation exists between $\Delta_{\text{r}}H$ and K_{d} .

reaction occurs in the volume where titrant enters the solution resulting in an exothermic heat effect. As titrant mixes into the solution and is diluted throughout the reaction vessel, some reverse reaction and the heat of dilution result in an endothermic heat effect. Close examination of the peaks near the end of the titration show these peaks indeed have an exotherm followed by an endotherm, see Fig. 5. Although a “ligand control” had been subtracted, this apparently did not exactly match the heat of dilution into the reaction mixture. Since the binding reaction

is not part of the blank, subtracting the average of the integral of peaks near the end of the titration from earlier peaks in the titration as is commonly done in determinations of K_d and $\Delta_r H$, causes a systematic overcorrection for Q_{dil} . We thus adopted the method illustrated in Fig. 5 to estimate the endothermic component as dQ_{dil}/dt , which was then subtracted from each injection. Note that this procedure for blank correction is unique to this data set and not a universal solution, which awaits future work. The resulting $dQ_{reaction}/dt$ curve could then be globally fit entirely within the random error band around the data as shown in Fig. 6. The results are given in Table 2.

Fig. 7 shows the correlations among the fitting parameters. The correlations show that τ is significantly correlated with k_{for} and k_{rev} . This result is expected since these three parameters are all described by similar exponential functions. This correlation reinforces the importance of including the time constant as a fitting parameter; using an incorrect value may accommodate a good fit, but lead to significant errors in the inferred kinetic parameters. Fig. 7 also shows that $\Delta_r H$ is significantly correlated with n . This result is expected since n describes the amount of reaction as calculated from the endpoint of the titration. As expected, K_d is correlated with the kinetic constants.

K_d and $\Delta_r H$ were also determined for the same data set with the NanoAnalyze program from TA Instruments, with the results shown in Table 2. The NanoAnalyze program first subtracts a baseline, integrates the area under each peak, and then by least squares minimization, simultaneously determines a constant blank to be subtracted from all peaks and values for K_d and $\Delta_r H$. Or, as an option, a constant blank value can be chosen to be subtracted from all the integrated peak areas. Since the blank is determined from the integrated areas of the peaks, this procedure is subject to the systematic error discovered during the global fit of the heat rate data as described above. Since the n value from NanoAnalyze differed slightly from that obtained from the global fit code, a global fit was run with n fixed at 0.847. The agreement between K_d from the global fit and K_d from NanoAnalyze validates the relation $K_d = k_{rev}/k_{for}$ for this case.

After the above effort was completed, DeLeeuw and Chaires provided us with their results from fitting the same data with the Origin program from MicroCal and the AFFINImeter software. The Origin program uses a similar procedure as the NanoAnalyze program, and therefore is expected to be subject to the same systematic error in the blank correction. The AFFINImeter software used a value of τ determined in a separate experiment by an injection of methanol (13 s). The AFFINImeter report is given in Supplement 2 and the DeLeeuw and Chaires results are summarized in Table 2. To assess the effects on K_d , $\Delta_r H$, k_{for} , and k_{rev} of the differing values of n and τ obtained from the other programs, the global fit was run with fixed values of $\tau = 13$ s and $n = 0.874$ obtained from the AFFINImeter results. The kinetics module in AFFINImeter has recently been modified to allow τ to also be used as a fitting parameter, but DeLeeuw and Chaires were unable to obtain results from the modified program. Note that the value for τ obtained from our global fit closely agrees in this case with the 13 s value supplied by DeLeeuw and Chaires.

The kinetic rate constants, k_{for} and k_{rev} , from all the different methods agree within the uncertainty limits of the global fit. The differences in K_d , $\Delta_r H$, and n trace back to differences in procedures and baseline and blank corrections. Note that in our procedure, K_d is computed last from the kinetic data. In the AFFINImeter procedure, K_d is computed first, and then used to obtain kinetic data [23]. As a consequence, the AFFINImeter results are subject to the systematic error caused by subtraction of an incorrect Q_{dil} . The traditional methods of blank correction cause a systematic error in the calculated K_d , n , and $\Delta_r H$ because it does not allow for the heat that is produced from the forward reaction. Some amount of forward reaction must occur after the apparent endpoint because the reaction is incomplete, i.e. K_d is relatively large, some free reactant remains in the reaction vessel, and reaction must occur when more titrant is added. The heat from this reaction is wrongly subtracted if the traditional method of blank correction is used.

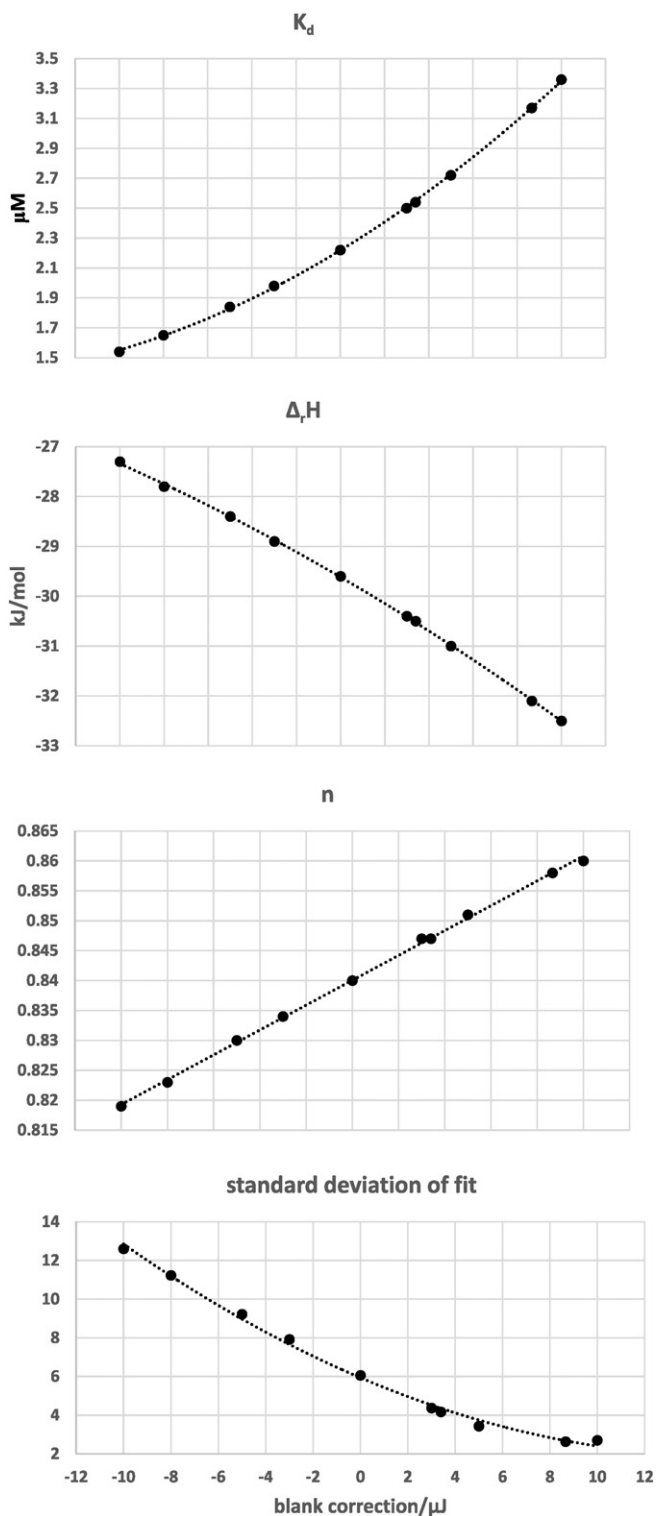


Fig. 8. The effect of variable Q_{dil} on derived values of $\Delta_r H$, K_d , n and the standard deviation of the fit with NanoAnalyze.

The large differences in n and Δ_rH in Table 2 between the AFFINImeter and Origin results are surprising and appear to be caused by differences in the way the baseline and blank corrections were done. Even though a ligand control was subtracted from the data, the blank Q_{dil} contains the systematic error as discussed above. This conclusion and the significance of the error was tested by fitting the integrated peaks with NanoAnalyze with differing constant blank corrections. The effects of differing blank values on Δ_rH , K_d , n and the standard deviation of the fit are shown in Fig. 8. Averaging the integral of the last three peaks gives a Q_{dil} of 3.0 μJ , averaging the integral of the last ten peaks gives a Q_{dil} of 3.4 μJ , and allowing Q_{dil} to float for a best fit with Δ_rH , K_d , and n as the other fitting parameters gives a Q_{dil} of 8.66 μJ . The other values on the horizontal axis in Fig. 8 were arbitrarily chosen to provide information on the shape of the response to variation in Q_{dil} . The response of n is linear while the responses of Δ_rH , K_d , and the standard deviation of the fit are all quadratic. Note that the results of the Origin analysis are beyond the range of blank correction values in Fig. 8, i.e. a Q_{dil} value of $-14 \mu J$ would be required to obtain the Origin values in Table 2. The reason for this discrepancy is apparently a difference in the $(dQ/dt)_{baseline}$ selected before the data were integrated. The value of $(dQ/dt)_{baseline}$ proportionally has a large effect on the value of the integral of the small peaks near the end of the titration curve. Thus we conclude that the procedures traditionally used for blank and baseline correction are not optimal and that the traditional way of analyzing the integrated data for Δ_rH , K_d , and n contains a systematic error that increases as ligand binding gets weaker. We note that for the case examined here, relative errors as large as $\pm 33\%$ in K_d , $\pm 20\%$ in Δ_rH , and $\pm 5\%$ in n can result from possible errors in Q_{dil} and $(dQ/dt)_{baseline}$.

Transparency Document

The Transparency document associated with this article can be found, in the online version.

Acknowledgments

Lynn DeLeeuw and Jonathan B. Chaires provided data and Origin and AFFINImeter analyses for the thermodynamics and kinetics of the binding reaction.

Appendix A. Supplementary data

Supplementary data to this article can be found online at <http://dx.doi.org/10.1016/j.bbagen.2015.12.018>.

References

[1] J. Chelieski, A.P. Citadini, H.J. Wiggers, A.J. Costa-Filho, M.C. Nonato, C. Montanari, Isothermal titration calorimetry as a tool for determining kinetic parameters of

- Trypanosoma cruzi* dihydroorotate dehydrogenase enzyme. Brazilian Chemical Society (SBQ). Division of Medicinal Chemistry, 4th Brazilian Symposium on Medicinal Chemistry, 2008.
- [2] M.J. Todd, J. Gomez, Enzyme kinetics determined using calorimetry: a general assay for enzyme activity? *J. Anal. Biochem.* 296 (2001) 179–187.
- [3] S.N. Olsen, Applications of isothermal titration calorimetry to measure enzyme kinetics and activity in complex solutions, *Thermochim. Acta* 448 (2006) 12–18.
- [4] B.A. Williams, E.J. Toone, Calorimetric evaluation of enzyme kinetic parameters, *J. Organomet. Chem.* 58 (1993) 3507–3510.
- [5] R. Ghaia, R.J. Falconer, B.M. Collins, Applications of isothermal titration calorimetry in pure and applied research—survey of the literature from 2010, *J. Mol. Recognit.* 25 (2012) 32–52.
- [6] N.A. Demarse, C. Quinn, D.L. Eggett, D.J. Russell, L.D. Hansen, Calibration of nanowatt isothermal titration calorimeters with overflow reaction vessels, *Anal. Biochem.* 417 (2011) 247–255.
- [7] C.W. Hansen, L.D. Hansen, A.D. Nicholson, M.C. Chilton, N. Thomas, J. Clark, J.C. Hansen, Correction for instrument time constant and baseline in determination of chemical kinetics, *In. J. Chem. Kinet.* 43 (2011) 53–61.
- [8] M.K. Transtrum, L.D. Hansen, C. Quinn, Enzyme kinetics determined by single-injection isothermal titration calorimetry, *Methods* 76 (2015) 194–200.
- [9] M. Goličnik, On the Lambert W function and its utility in biochemical kinetics, *Biochem. Eng. J.* 63 (2012) 116–123.
- [10] C. Aguirre, I. Condado-Morales, L.F. Olguin, M. Costas, Isothermal titration calorimetry determination of individual rate constants of trypsin catalytic activity, *Anal. Biochem.* 479 (2015) 18–27.
- [11] S.N. Olsen, E. Lumby, K.C. McFarland, K. Borch, P. Westh, Kinetics of enzymatic high-solid hydrolysis of lignocellulosic biomass studied by calorimetry, *Appl. Biochem. Biotechnol.* 163 (2011) 626–635.
- [12] N. Barros, V. Piñeiro, L.D. Hansen, P. Vikegard, Calorimetry measures the response of soil organic matter biodegradation to increasing temperature, *J. Therm. Anal. Calorim.* (2015) <http://dx.doi.org/10.1007/s10973-015-4947-8>.
- [13] R.B. Kemp (Ed.), *Handbook of thermal analysis and calorimetry, From Macromolecules to Man, Vol. 4*, Elsevier, Amsterdam, 1999.
- [14] L.D. Hansen, N.R. Thomas, B. Arnholt-Schmitt, Temperature responses of substrate carbon conversion efficiencies and growth rates of plant tissues, *Physiol. Plant.* 137 (2009) 446–458.
- [15] V.S. Mukhanov, L.D. Hansen, R.B. Kemp, Nanocalorimetry of respiration in microorganisms in natural waters, *Thermochim. Acta* 531 (2012) 66–69.
- [16] P. Závodszy, J. Kardos, Á. Svingor, G.A. Petsko, Adjustment of conformational flexibility is a key event in the thermal adaptation of proteins, *Proc. Natl. Acad. Sci. U. S. A.* 95 (1998) 7406–7411.
- [17] G. Žoldák, R. Šuták, M. Antalík, M. Sprinzl, E. Sedlák, Role of conformational flexibility for enzymatic activity in NADH oxidase from *Thermus thermophilus*, *Eur. J. Biochem.* 270 (2003) 4887–4897.
- [18] D.T. Haynie, *Biological Thermodynamics*, second ed. Cambridge University Press, Cambridge, 2008 231.
- [19] W.L. Ng, Thermal decomposition in the solid state, *Aust. J. Chem.* 28 (1975) 1169–1178.
- [20] L.D. Hansen, E.A. Lewis, D.J. Eatough, R.G. Bergstrom, D. DeGraft-Johnson, Kinetics of drug decomposition by heat conduction calorimetry, *Pharm. Res.* 6 (1988) 20–27.
- [21] L.D. Hansen, Calorimetric measurement of the kinetics of slow reactions, *Ind. Eng. Chem. Res.* 39 (2000) 3541–3549.
- [22] T. Egawa, A. Tsuneshige, M. Suematsu, T. Yonetani, Method for determination of association and dissociation rate constants of reversible bimolecular reactions by isothermal titration calorimeters, *Anal. Chem.* 79 (2007) 2972–2978.
- [23] D. Burnouf, E. Ennifar, S. Guedich, B. Puffer, G. Hoffmann, G. Bec, F. Disdier, M. Baltzinger, P. Dumas, kinTC: a new method for obtaining joint thermodynamic and kinetic data by isothermal titration calorimetry, *J. Am. Chem. Soc.* 134 (2012) 559–565.
- [24] <https://www.affinimeter.com/> accessed 26 June 2015.